Effect of Receptor-Ligand Affinity on the Strength of Endothelial Cell Adhesion

Yao Xiao* and George A. Truskey*#
*Center for Biochemical Engineering and #Department of Biomedical Engineering, Duke University, Durham, North Carolina 27708 USA

ABSTRACT The objective of this study was to determine the effect of receptor-ligand affinity on the strength of endothelial cell adhesion. Linear and cyclic forms of the fibronectin (Fn) cell-binding domain peptide Arg-Gly-Asp (RGD) were covalently immobilized to glass, and Fn was adsorbed onto glass slides. Bovine aortic endothelial cells attached to the surfaces for 15 min. The critical wall shear stress at which 50% of the cells detached increased nonlinearly with ligand density and was greater with immobilized cyclic RGD than with immobilized linear RGD or adsorbed Fn. To directly compare results for the different ligand densities, the receptor-ligand dissociation constant and force per bond were estimated from data for the critical shear stress and contact area. Total internal reflection fluorescence microscopy was used to measure the contact area as a function of separation distance. Contact area increased with increasing ligand density. Contact areas were similar for the immobilized peptides but were greater on surfaces with adsorbed Fn. The dissociation constant was determined by nonlinear regression of the net force on the cells to models that assumed that bonds were either uniformly stressed or that only bonds on the periphery of the contact region were stressed (peeling model). Both models provided equally good fits for cells attached to immobilized peptides whereas the peeling model produced a better fit of data for cells attached to adsorbed Fn. Cyclic RGD and linear RGD both bind to the integrin $\alpha_V\beta_3$, but immobilized cyclic RGD exhibited a greater affinity than did linear RGD. Receptor affinities of Fn adsorbed to glycophase glass and Fn adsorbed to glass were similar. The number of bonds was calculated assuming binding equilibrium. The peeling model produced good linear fits between bond force and number of bonds. Results of this study indicate that 1) bovine aortic endothelial cells are more adherent on immobilized cyclic RGD peptide than linear RGD or adsorbed Fn, 2) increased adhesion is due to a greater affinity between cyclic RGD and its receptor, and 3) the affinity of RGD peptides and adsorbed Fn for their receptors is increased after immobilization.

INTRODUCTION

Endothelial cell seeding of synthetic vascular grafts represents a promising approach to reduce thrombogenicity and intimal hyperplasia (Williams et al., 1994). To minimize the likelihood of infection, seeding and implantation must occur quickly (Williams et al., 1994). Strong adhesion must develop rapidly for cells to resist forces exerted by flowing blood. Adhesion is enhanced by incubating the graft with the recipient's plasma (Rupnick et al., 1989), adsorbing adhesion proteins such as fibronectin (Fn), vitronectin (Vn), or laminin (Dekker et al., 1993), or covalently immobilizing peptide sequences containing the cell-binding domains of Fn (RGD) or laminin (YIGSR) (Massia and Hubbell, 1990, 1991; Nicol et al., 1992). Immobilized peptides create a uniform and reproducible surface and eliminate possible immunological reactions.

Due to limited time available for endothelial cells to attach and spread on graft surfaces in a clinical environment, factors that promote rapid and strong adhesion need to be examined. Altering receptor-ligand affinity represents one approach to increase the strength of adhesion of endothelial cells to vascular grafts. In solution, the affinity of Fn for its integrin receptor $\alpha_5\beta_1$ (10^{-6} M) (Akiyama and Yamada, 1985) is greater than the affinity of linear (10^{-3} M) RGD peptides for the Vn integrin receptor $\alpha_V\beta_3$ (Pierschbacher and Ruoslahti, 1987). Cyclization constrains the RGD conformation, which increases the peptide affinity for the integrin $\alpha_V\beta_3$ (Pierschbacher and Ruoslahti, 1987). The affinity of RGD peptides for integrins also depends upon amino acids flanking the RGD sequence and spacer groups linking the peptide to the surface (Craig et al., 1995). Interestingly, covalently immobilized linear RGD peptides promoted cell spreading and focal contact formation at lower densities than occurred with adsorbed Fn (Massia and Hubbell, 1991). This observation suggests that the affinities of immobilized RGD peptides may be greater than when the peptides are in solution.

Surface properties affect the conformation of adsorbed adhesion proteins and protein-receptor affinity (Giroux and Cooper, 1990; Grinnell and Feld, 1982). To evaluate the significance of these observations upon cell adhesion, we examined the effect of surface hydrophobicity on endothelial cell adhesion to adsorbed Fn (Iuliano et al., 1993). The cell-binding domain of Fn exists in different conformations when Fn is adsorbed on surfaces with different hydrophobicity. Changes in the strength of cell adhesion suggested that conformation could affect the affinity of Fn for its receptor. In addition to conformational changes upon adsorption, Fn may adsorb in a variety of orientations, some of which render the cell-binding domain inaccessible to its

Received for publication 27 December 1994 and in final form 23 August 1996.

Address reprint requests to Dr. George A. Truskey, Department of Biomedical Engineering, Duke University, Box 90281, Durham, NC 27708-0281. Tel.: 919-660-5147; Fax: 919-660-5362; E-mail: gtruskey@acpub.duke.edu.

0006-3495/96/11/2869/16 $2.00

receptor (Garrison et al., 1992; Iuliano et al., 1993). Consequently, attributing changes in adhesion strength to changes in conformation are more complicated for adsorbed proteins than with peptides covalently immobilized in the same orientation (Massia and Hubbell, 1991).

The objective of the current study was to test the hypothesis that the conformation and accessibility of immobilized ligand affect the strength of adhesion. Cell adhesion and control peptides were covalently immobilized on surfaces via the terminal amine (Massia and Hubbell, 1990, 1991). Peptides used were linear RGD, cyclic RGD, and a nonadhesive control peptide. Fn was adsorbed from solution. Adhesion strength was determined by exposing adherent bovine aortic endothelial cells (BAECs) to steady laminar flow and measuring cell detachment as a function of wall shear stress. The net hydrodynamic force exerted on a cell was calculated using a two-dimensional numerical model (Olivier and Truskey, 1993). The contact area between cell membrane and substratum was measured by total internal reflection fluorescence microscopy (TIRFM). These results were used to compute the receptor-ligand dissociation constant and the force per bond for cells adherent to immobilized RGD peptides and adsorbed Fn.

MATERIALS AND METHODS

Covalent immobilization of RGD

Peptides were immobilized onto glass slides via the terminal amine using the procedure of Massia and Hubbell (1990). Clean glass slides (Clay Adams, Becton Dickinson, Franklin Lakes, NJ) were soaked in 0.5 N NaOH for 2 h, rinsed with deionized water, and immersed in an aqueous solution of 1% (3-glycidoxypropyl)-trimethoxysilane (Sigma Chemical Co., St. Louis, MO), pH 5.5. The solution was maintained at 90°C for 2 h and then washed with deionized water. Slides were baked with 1 mM HCl at 90°C for 1 h to convert the oxirane groups to glycol groups (glycophase glass). Dried glycophase glass slides were rinsed with acetone dried over molecular sieve 4A (Fisher Scientific, Pittsburgh, PA). In 1 ml of dry acetone, 200 μl of dry pyridine (Aldrich Chemical Co., Milwaukee, WI) and 100 μl of dry 2,2,2-trifluoroethanesulfonyl chloride (tresyl chloride, Fluka Chemical Corp., Ronkonkoma, NY) were mixed and added to the upper surface of each glycophase slide. The reaction proceeded for 15 min at room temperature. Slides were rinsed with 1 mM HCl and 0.2 M sodium bicarbonate solution.

The linear RGD peptide (Gly-Arg-Gly-Asp-Ser-Pro), cyclic RGD peptide (Gly-Pen-Gly-Arg-Gly-Asp-Ser-Pro-Cys-Ala where Pen is penicillamine and a disulfide bond links penicillamine and cysteine), and the control peptide GRADSP (Gly-Arg-Ala-Asp-Ser-Pro) (Telios Pharmaceuticals, San Diego, CA) were added to 0.2 M sodium bicarbonate (pH 10.0; coupling buffer) at concentrations from 4.3 fmol/ml to 21 pmol/ml. Tresyl-chloride-activated slides were rinsed with coupling buffer and a stoichiometric amount of the peptide solution was added on the upper surface of the slides. The reaction proceeded for 20 h at room temperature. Only primary and secondary amines react with tresyl-chloride-activated glycophase glass (Massia and Hubbell, 1992). Slides were rinsed with deionized water and coupling buffer. β-Mercaptoethanol breaks the disulfide bond in the cyclic RGD peptide and was not used to block unreacted sites (Massia and Hubbell, 1990). Instead, the GRADSP-grafted surfaces were used to correct for nonspecific adhesion.

Surface densities of RGD peptides were estimated using the correlation between input peptide concentration and immobilized surface concentration for radiolabeled GRGDSY peptides (Massia and Hubbell, 1990). The amount immobilized per unit area is stoichiometrically related to the amount of peptide supplied per unit surface area and limited by the amount of peptide provided when the peptide in solution is less than or equal to 12.1 pmol/(cm^2 glass) (Massia and Hubbell, 1990). For RGD- or RAD-containing peptides with input densities of 0.0038 pmol/cm^2, 0.058 pmol/cm^2, and 3.8 pmol/cm^2, the corresponding ligand surface densities were 2.3×10^9 molecules/cm^2, 2.3×10^{10} molecules/cm^2, and 2.3×10^{12} molecules/cm^2, respectively.

Fibronectin adsorption

Fn was isolated from fresh human plasma by gelatin-agarose affinity chromatography (Ruoslahti et al., 1988) and equilibrated with 0.1 M NaCl and 50 mM Tris (pH 7.4) by dialysis. Purity was assessed by sodium dodecyl sulfate polyacrylamide gel electrophoresis. The Fn concentration was determined from the absorbance at 280 nm with a molar extinction coefficient of 1.28 cm^2/mg. The Fn solution was divided into aliquots and stored in liquid nitrogen until used.

To adsorb proteins, clean glass or glycophase glass slides were incubated with 0.1, 1, or 10 μg/ml Fn for 1 h at room temperature. The solution was removed and slides were rinsed twice in sterile deionized water and used immediately. The surface density of adsorbed ^{125}I-labeled Fn was measured according to the protocol of Truskey and Pirone (1990) and is summarized in Table 1.

Surface characterization

Clean glass, glycophase glass, and peptide-derivatized surfaces were analyzed by x-ray photoelectron spectroscopy (XPS) (Department of Chemistry, the University of North Carolina at Chapel Hill, Chapel Hill, NC). Analysis was conducted with a Physical Electronics PHI 5400 system using a magnesium x-ray source (1253.6 eV) at a pressure of approximately 1×10^{-8} torr and a 1-mm spot size. A survey scan was performed to identify all elements present. Higher resolution scans were then performed to obtain quantitative information. Binding energies were corrected by referencing to the main carbon 1s line at 285.0 eV.

Cell cultivation

BAECs were isolated from fresh calf aortas by mechanical scraping. BAECs were dipped in cell culture medium consisting of Dulbecco's modified Eagle's medium (DMEM; Sigma) with 10% fetal calf serum, 2 μmol/ml glutamine, 100 U/ml penicillin, and 100 μg/ml streptomycin and then centrifuged at 1500 rpm for 10 min at 4°C. Cells were resuspended in 10 ml of cell culture medium in 75-cm^2 cell culture flasks. For experiments, cells were used in passages 2 to 12.

For an experiment, endothelial cells were rinsed twice with Hanks' buffered saline solution (Sigma) without Ca^{2+} and Mg^{2+}. Cells were incubated with 1 mM EGTA in phosphate-buffered saline for 15 min at 37°C followed by centrifugation at 1500 rpm for 10 min at 4°C. To investigate the effect of proteolytic cleavage of integrins on the strength of adhesion, cells were incubated with 0.05% trypsin, 0.53 mM EDTA for 10 min at 37°C. Detached cells were resuspended in DMEM containing 1% (w/v) bovine serum albumin. Cells were incubated with surfaces at 37°C in a humidified 5% CO_2/95% air atmosphere for 15 min.

TABLE 1 Adsorbed fibronectin concentrations on glass and glycophase surfaces

Fn concentration (μg/ml)	Amount adsorbed (ng/cm^2)	
	Glass	Glycophase glass
0.1	2.54 ± 0.05 (n = 5)	3.0 ± 2.0 (n = 5)
1.0	25.4 ± 0.5 (n = 5)	22.0 ± 8.0 (n = 5)
10	148 ± 2.0 (n = 5)	45 ± 14 (n = 5)

Flow experiments

The variable-height flow chamber consists of a narrow gasket of thickness H_o with the upper surface inclined at an angle α (Fig. 1). H_o was either 0.0254 cm or 0.0508 cm. In one experiment, a 0.1016-cm-thick gasket was used. The entrance length was 2.54 cm followed by a working length L (5.08 cm) and an exit length of 2.54 cm. The channel width w was 1.4 cm. The inclined surface was milled into a plexiglass plate and $h(x)$ was measured with a micrometer. Because of the small angle of inclination (α = 0.3235°), inertial effects in the vertical direction were small and the velocity profile was parabolic (Denn, 1980).

One-dimensional flow was approximated with width-to-height ratios between 11.4 and 29.8. Based upon the solution for two-dimensional flow in a rectangular channel (Batchelor, 1967), these width-to-height ratios produce average wall shear stresses within 1.5 and 0.5%, respectively, of the value for one-dimensional flow.

For a rectangular channel, the entrance length equals $0.08hRe$ (Schlichting, 1979), where the Reynolds number (Re) for a channel is $Re = 2Q/\nu(w + h)$; Q is the volumetric flow rate, and ν is the kinematic viscosity. The largest Reynolds number obtained in this study was 250 for which the entrance length was 0.94 cm. This entrance length was less than the entrance length for the flow chamber. Thus, flow could be approximated as one dimensional and fully developed.

Flow rates between 1.5 and 3.5 $cm^3\ s^{-1}$ were generated by a gravity feed from a reservoir maintained at 37°C. For unreacted glycophase surfaces an infusion pump was used to introduce the fluid through a 20-cm^3 syringe with a flow rate of 0.129 $cm^3\ s^{-1}$. Viscosities were measured with either a cone and plate viscometer (Brookfield Engineering Laboratories, Stoughton, MA) or a couette viscometer (Rheometric Scientific, Piscataway, NJ). For shear stresses below 100 dyne cm^{-2}, the medium consisted of DMEM that was Newtonian with a viscosity of 0.0085 g $cm^{-1}\ s^{-1}$ at 37°C. For a Newtonian fluid, the wall shear stress τ_w (dyne cm^{-2}) is (Truskey and Pirone, 1990)

$$\tau_w = \frac{6\mu Q}{wh(x)^2}, \tag{1}$$

where μ is the fluid viscosity at 37°C, and Q is the volumetric flow rate. Wall shear stresses ranged from 0.6 to 150 dyne cm^{-2}.

At the highest cyclic RGD density a solution of 3% dextran (molecular weight, 2×10^6; Sigma) in DMEM was used to increase the viscosity. This dextran solution exhibited a slight deviation from a Newtonian fluid and was well fit to the power law model (r = 0.91, $0.0002 < p < 0.0005$):

$$\eta_{app} = \eta_o \dot{\gamma}^{n-1}, \tag{2}$$

where $\dot{\gamma}$ is the shear rate. For shear rates between 9 s^{-1} and 750 s^{-1} η_o = 0.046 ± 0.005 g $cm^{-1}\ s^{-1}$ and n = 0.979 ± 0.003 g $cm^{-1}\ s^{-1}$. The value of n was significantly different than one ($p < 0.001$). The maximal shear rate produced in the flow chamber was 3200 s^{-1}. Due to the presence of secondary flows in the viscometers, viscosity was not determined for shear rates above 750 s^{-1}. For a power law fluid in the variable-height flow chamber, the wall shear stress is calculated as

$$\tau_w = \frac{2\eta_o(2n + 1)Q}{wh(x)^2}. \tag{3}$$

Slides with cells were mounted in the flow chamber and exposed to flow for 4–7 s. This time period was chosen based upon previous studies (Truskey and Pirone, 1990; Truskey and Proulx, 1993) that showed that cell detachment was biphasic with most cell loss occurring immediately after the onset of flow. For flow in a channel, the time to reach steady state is approximately $h^2\rho/4\nu$ (Bird et al., 1960). For conditions used in this study, the time to reach steady state ranged from 0.019 to 0.45 s, which amounts to less than 10% of the time cells were exposed to flow.

The number of adherent cells before and after flow was counted at five equally spaced positions along the flow chamber, and the fraction of adherent cells was obtained. Cell areas were measured by image analysis (Truskey and Pirone, 1990). A minimum of 100 cells were analyzed for each condition.

Because of the heterogeneity of the cell surface receptor density and contact size among the cell population, cells exhibit a distribution of adhesive stresses, which is well described by a log-normal distribution (Iuliano et al., 1993). The critical shear stress (τ_c), which is the shear stress required to detach 50% of the cells from the surface, was determined by nonlinear regression (Bates and Watts, 1988) of the log-normal distribution to cell detachment data.

Total internal reflection fluorescence microscopy

The separation distance of the basal surface of the cell from the substrate was measured by TIRFM. The total internal reflection of visible light at the solid/liquid interface produces an exponentially decaying evanescent wave that excites fluorescence within a few tenths of a micron into the liquid phase (Reichert, 1989). For the case of a membrane containing a fluor, fluorescence intensities $F(x, y)$ are related to the separation distance from cell membrane and substratum $\Delta(x, y)$ as follows (Reichert and Truskey, 1990):

$$\Delta(x, y) = \Delta_o + d_p \ln[F_o/F(x, y)], \tag{4}$$

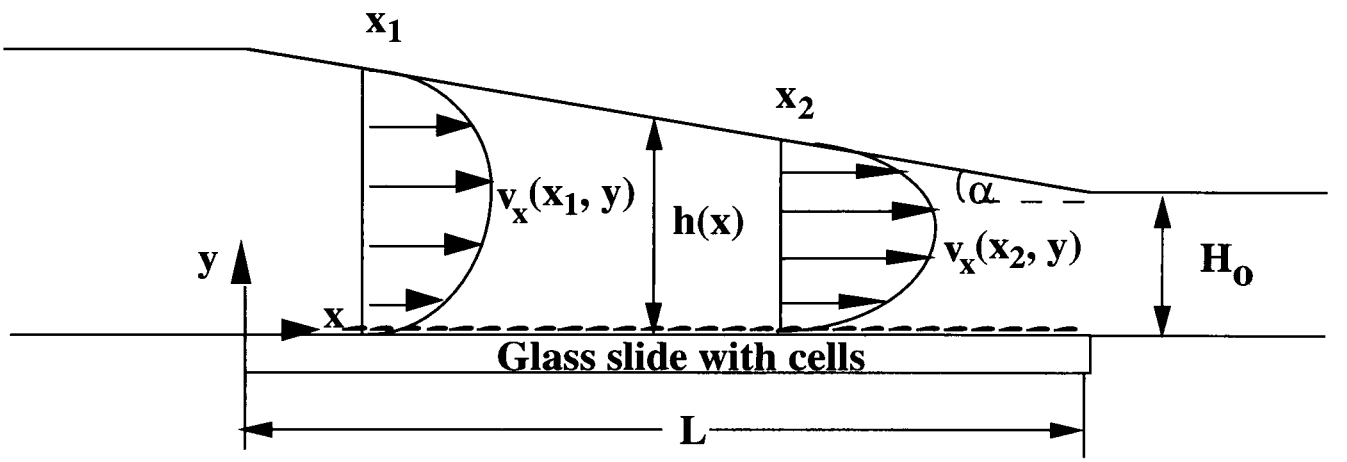

FIGURE 1 Schematic diagram of the variable-height laminar flow chamber. Cells attach to a glass slide on the lower surface. Fluid flows though a gap of height h that varies linearly with position. The angle of inclination (α = 0.3235°) is sufficiently small such that inertial effects in the vertical direction are small and the velocity profile is parabolic. The local wall shear stress is given by Eq. 1 for a Newtonian fluid and Eq. 3 for a power law fluid.

where F_o is the maximal image brightness corresponding to the minimal membrane substratum separation Δ_o, and d_p (101.5 nm) is the depth of penetration of the evanescent wave at the laser incident angle of 70°. Electron microscopy studies indicate a focal contact separation distance of 10–15 nm (Chen and Singer, 1982), and variable angle TIRFM yielded a value of 24 ± 13 nm (Burmeister et al., 1994). RGD peptides grafted on glycophase glass are approximately 2–3 nm long and the receptors protrude 20–23 nm from the cell membrane (Hynes, 1992). Based upon these considerations the minimal separation distance Δ_o is assumed to be between 10 and 25 nm.

Fixed, adherent BAECs were labeled with 3 g/l 1,1′-dioctadecyl-3,3,3′,3′-tetramethyl-indocarbo-cyanineperchlorate ($DiIC_{18}(3)$; Molecular Probes, Eugene, OR) (Truskey et al., 1992). A glass slide with adherent cells was placed in the TIRF flow cell. A truncated hemicylindrical prism (BK-7 glass, n = 1.522, Harrick Scientific, Ossining, NY) was optically coupled to the microscope slide using type DF immersion oil (n = 1.518 ± 0.002; Cargille, Cedar Grove, NJ). The evanescent wave was produced using 514.5-nm light from an Ar^+ laser (Ion Laser, Salt Lake City, UT). The flow cell was centered in the optical axis of the microscope by aligning the epifluorescence optics and objective of the microscope with the central axis of the hemicylindrical prism. TIRFM and epifluorescence images were collected with a 100× objective and imaged onto a thermoelectrically cooled Star 1 CCD camera (Photometrics, Tucson, AZ) to produce a digitized map of image intensities. Calculation of the separation contours from Eq. 4 was performed on a Silicon Graphics Indigo workstation using Matlab software (The MathWorks, Natick, MA). The contact area represented the membrane surface closer than the critical relative separation distance ($\Delta(x, y) - \Delta_o$).

Estimation of critical separation distance

The contact area represents the region over which bonds form between adhesion proteins and their receptors. For this analysis, the receptor-ligand complexes are treated as springs (Dembo et al., 1988; Ward and Hammer, 1993). The unstressed receptor-ligand complex length equals Δ_o. Stressing the receptor-ligand complex alters the equilibrium dissociation constant K_D as follows (Dembo et al., 1988; Ward and Hammer, 1993):

$$K_D = K_{D_o}\exp\left[\frac{\kappa(\Delta(x, y)-\Delta_o)^2}{2kT}\right], \quad (5)$$

where K_{Do} is the dissociation constant for unstressed bonds, κ is the spring constant, k is Boltzmann's constant, and T is the absolute temperature. Estimates of the spring constant of Fn, Vn, and their integrin receptors range from 0.1 to 1 dyne cm^{-1} (Dembo et al., 1988; Erickson, 1994). The bond density N_{LR} is found by solving the following equilibrium relationship:

$$K_D = \frac{(N_{R_o}-N_{LR})(N_{L_o}-N_{LR})}{N_{LR}}, \quad (6)$$

where N_{Ro} and N_{Lo} are the initial receptor and ligand densities, respectively.

Solutions to Eqs. 5 and 6 for the bond density were examined over the expected range of ligand and receptor densities, spring constants, and unstressed equilibrium constants. For increases of less than 3 nm beyond Δ_o, the bond density decreased slightly (Fig. 2 *A*). At larger separation distances, the bond density declined dramatically with small increases in separation distance. The critical separation distance (Δ_{crit}) represents the relative separation distance at which the bond density declined to 50% of its maximal value ($N_{LR0.5\ max}$). This quantity was calculated from Eqs. 5 and 6:

$$\Delta_{crit} = \sqrt{\frac{2kT}{\kappa}\ln(K_{D_o}/N_{LR_{0.5max}})}, \quad (7a)$$

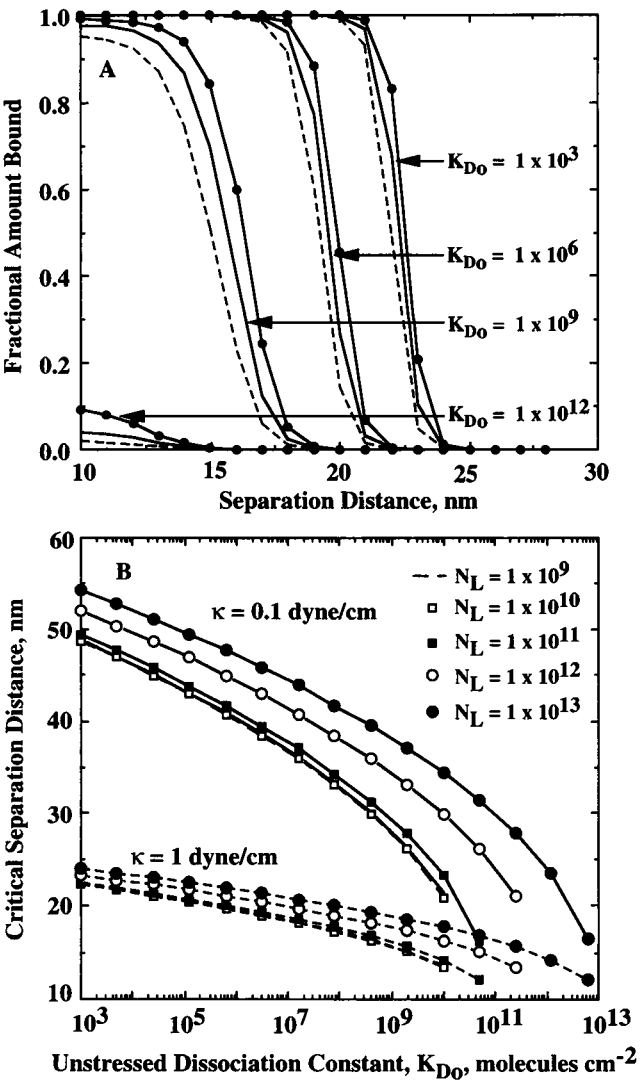

FIGURE 2 (*A*) Effect of unstressed equilibrium constant upon the change in the bond density with separation distance for N_{Lo} = 1 × 10^9 molecules cm^{-2}, κ = 1 dyne cm^{-1}, and N_{Ro} = 2 × 10^{10} molecules cm^{-2} (- - -), 4.4 × 10^{10} molecules cm^{-2} (——), and 10 × 10^{10} molecules cm^{-2} (—●—). (*B*) Critical separation distance (Δ_{crit}) as a function of ligand-receptor K_{Do} and ligand density for spring constants of 0.1 and 1 dyne cm^{-1}.

where

$$N_{LR_{0.5max}} = 0.25\{(K_{D_o} + N_{L_o} + N_{R_o}) - \sqrt{(K_{D_o} + N_{L_o} + N_{R_o})^2 - 4N_{L_o}N_{R_o}}\} \quad (7b)$$

In general, the critical separation distance decreased as the spring constant increased and as the unstressed equilibrium constant increased (Fig. 2 *B*).

Hydrodynamic analysis of forces on cells exposed to flow

For a given critical shear stress, the net hydrodynamic force exerted on the cell, F_T, was found using two-dimensional numerical solutions of the velocity and stress fields (Olivier and Truskey, 1993). Cells were treated as

rigid bodies with constant volume based upon light microscope observation at ×200 that the shape and projected area did not change after 20 s of exposure to shear stresses as high as 53 dyne cm^{-2} (Truskey and Proulx, 1993). The shapes represented adherent BAECs at different stages of spreading and adhesion. Force balances in the x and y directions are (Fig. 3)

$$\sum F_x = F_{xs} + \int_{-a}^{a} N_{LR} f_{bx}(x)dx = 0 \qquad (8a)$$

$$\sum F_y = F_{ys} + \int_{-a}^{a} N_{LR} f_{by}(x)dx = 0, \qquad (8b)$$

where F_{xs} and F_{ys} are the drag and lift forces per unit length, a is the radius of the base of the cell, and f_{bx} and f_{by} are the bond forces acting in the x and y directions, respectively. In general, F_{ys} is not zero and slightly more than one-half of the bonds are compressed. The force resultants act at $\bar{x}$, $\bar{y}$ (Fig. 3). A moment balance performed about the origin yields

$$\sum M_o = T_{zs} + \int_{-a}^{a} N_{LR} f_{by}(x)xdx = 0, \qquad (9)$$

where T_{zs} is the hydrodynamic torque per unit length acting on the cell ($T_{zs} = F_{ys}\bar{x} + F_{xs}\bar{y}$).

Determination of the force per bond requires solution of the detailed mechanics of membrane and bond deformation (Evans, 1985; Ward and Hammer, 1993). Because of the complex shape of the cell and lack of information regarding the rheological properties of adherent endothelial cells, two simplified models were used for the bond stress distribution (Olivier and Truskey, 1993): the uniform stress model (Hammer and Lauffenburger, 1987) and the peeling model (Ward and Hammer, 1993).

In the uniform stress model, bonds are stressed or compressed to the same extent and Eqs. 8a, 8b, and 9 reduce to

$$F_{xs} = -2aN_{LR} f_{bx} \qquad (10a)$$

$$F_{ys} = 2LN_{LR} f_{by} \qquad (10b)$$

$$T_{zs} = L^2 N_{LR} f_{by} + a^2 N_{LR} f_{by}, \qquad (10c)$$

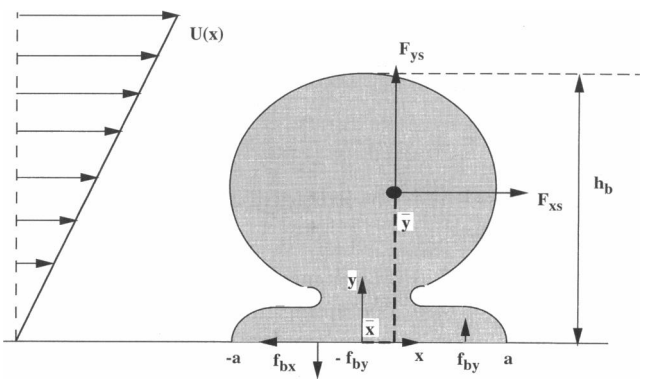

FIGURE 3 Schematic of forces acting on a cell of height h_b exposed to a laminar shear flow. The base of the cell has radius a. The flow exerts force components F_{xs} and F_{ys} that are resisted by forces f_{bx} and f_{by} exerted by receptor-ligand bonds.

where L is where f_{by} switches from compression to tension. Eliminating L from Eqs. 10b and 10c and solving for the net force exerted on the cells ($F_T = N_{LR}A_c f_b = N_b A_c |f_{bx}^2) + f_{by}^2|^{1/2}$) yields

$$F_T = [a^2F_{xs}^2 + a^2F_{ys}^2 + 2T_{zs}^2 + 2T_{zs}\sqrt{a^2F_{ys}^2 + T_{zs}^2}]^{1/2}, \qquad (11)$$

where a is the radius of the cell region in contact with the surface. Eq. 11 converts the forces per length into units of force by multiplying by the radius of the base of the cell. As cells were in the early stages of spreading, cell shape 2 (Olivier and Truskey, 1993) was used (Fig. 3). The cell height is 12 μm and the cell radius is 6 μm. F_{xs} and T_{zs} were obtained using (Olivier and Truskey, 1993)

$$F_{xs} = 8.61 \times 10^{-3}\tau_c \qquad (12a)$$

$$T_{zs} = 7.56 \times 10^{-6}\tau_c. \qquad (12b)$$

The lift force per unit length F_{ys} was calculated from the following relation for cell 2:

$$F_{ys} = 4.42 \pm 0.31 \times 10^{-3}\tau_c - 4.54 \pm 0.41 \times 10^{-5}\tau_c^2 \qquad (12c)$$

The applicability of two-dimensional models was assessed by comparing the net hydrodynamic force for low Reynolds number flow over a sphere touching a surface (Goldman et al., 1967a,b) and a hemisphere in contact with a surface (Hyman, 1972) with the corresponding two-dimensional cases (Olivier and Truskey, 1993). For two-dimensional shapes, FIDAP was used to obtain the stress distribution over the cell surface from which the drag and lift forces and torque were determined. Eq. 11 was used to calculate the net force. The net forces differed by less than 5% for the corresponding two- and three-dimensional shapes.

Determination of the unstressed dissociation constant and force per bond

The unstressed dissociation constant (K_{Do}) and average force per bond were calculated using a modification of the procedure of Kuo and Lauffenburger (1993). For a range of ligand and receptor densities, equilibrium thermodynamics (see Appendix) was used to derive a general relation for the critical tension at which cells begin to detach (Eq. A8). This result is valid for all ligand densities and reduces to previously reported results at low and high ligand densities (Dembo et al., 1988; Ward and Hammer, 1993).

Using the analogy with Young's equation, the adhesive energy density γ is

$$\gamma = T_{crit}(1 + \cos\theta), \qquad (13)$$

where θ is the macroscopic contact angle between the cell membrane and the surface. The work required to separate the active sites of the receptor and ligand by the bond interaction distance l_b is approximately (Evans, 1985)

$$\gamma = \frac{N_{LR} f_b l_b}{2}, \qquad (14)$$

where f_b is the force per bond. The bond interaction distance represents the distance over which the noncovalent interaction between receptor and ligand occurs and is much smaller than the separation distance between the cell and substrate (Alon et al., 1995). A value of 1×10^{-7} cm was used for l_b (Bell, 1978; Kuo and Lauffenburger, 1993).

In the absence of nonspecific forces, the total bond force equals the net hydrodynamic force on the cell, F_T:

$$F_T = N_{LR} f_b A_c, \qquad (15)$$

where A_c is the contact area. Solving for the net hydrodynamic force yields

$$F_T = \frac{2kTA_c}{l_b}\left\{-N_{LR} + N_{R_o}\ln\left[\frac{N_{R_o}}{(N_{R_o}-N_{LR})}\right] + N_{L_o}\ln\left[\frac{N_{L_o}}{(N_{L_o}-N_{LR})}\right]\right\}. \quad (16)$$

For the peeling model, only bonds in the periphery of the contact region are stressed at any time (Evans, 1985; Kuo and Lauffenburger, 1993). The distance stressed δ was assumed to equal the distance between bonds, which was estimated assuming a square array of bonds:

$$\delta = \sqrt{1/N_{LR}} \quad (17)$$

For the peeling model, the contact area in Eq. 15a and 15b is replaced with the stressed area A_s:

$$A_s = A_c - \pi(a - \delta)^2 \quad (18)$$

The unstressed equilibrium constant as well as the spring constant and initial receptor density were determined by nonlinear regression (Bates and Watts, 1988) of data to Eqs. 6, 7, and 16 for net force as a function of ligand density as follows. To determine the component of adhesion due to receptor-ligand interactions, the critical shear stress produced by nonspecific adhesion in the absence of immobilized RGD or adsorbed Fn was subtracted from each data set. The net force as a function of ligand density was calculated from data for the critical wall shear stress using Eqs. 11 and 12. For each surface, the contact area as a function of separation distance was fit to a polynomial. The critical separation distance was then used to determine the contact area for the uniform stress model. The net force was calculated from Eq. 16. An iterative Marquardt method (Bates and Watts, 1988) was used to minimize the sums of squares of residuals between the theoretical and experimental values of total force and find the best fit value of K_{D_o}, κ, and N_{R_o}.

As linear and cyclic RGD bind to the integrin $\alpha_v\beta_3$ whereas fibronectin binds to the integrin $\alpha_5\beta_1$ (Massia and Hubbell, 1991; Pierschbacher and Ruoslahti, 1987), data for immobilized RGD peptides and adsorbed Fn were fit by the method of incremental parameters (Bates and Watts, 1988). For this approach, the spring constant was the same for immobilized RGD peptides and adsorbed Fn, different receptor densities were used for immobilized RGD peptides and adsorbed Fn, and a different affinity constant was used for each ligand. An analysis of variance of the extra sums of squares due to different affinity constants or receptor densities was used to evaluate whether the differences were statistically significant (Bates and Watts, 1988).

A range of values for the spring constant and receptor number are available. This information was incorporated into the regression by constraining the spring constant between 0.1 and 2 dyne cm^{-1} (Dembo et al., 1988; Erickson, 1994). The receptor number ranges from 500,000 receptors/cell for $\alpha_5\beta_1$ (Akiyama and Yamada, 1985) to 3×10^6 receptors/cell for $\alpha_v\beta_3$ (Conforti et al., 1989; Preissner et al., 1988). The total cell surface area is 2250 ± 60 μm^2 (Olivier and Truskey, 1993) yielding receptor densities from 2×10^{10} to 13×10^{10} receptors/cm^2. Likewise, the receptor density was constrained between 0.5×10^{10} and 10×10^{10} molecules/cm^2.

The unstressed dissociation constants were converted from units of molecules cm^{-2} to a three-dimensional value (K'_D, mol L^{-1}) as follows:

$$K'_D = K_D \frac{1000\ \text{cm}^3\ \text{liter}^{-1}}{6.02 \times 10^{23}\ \text{molecules mole}^{-1} - l\ \text{cm}} \quad (19)$$

where l is the depth at which the soluble ligands are available to the surface. For l equal to 2×10^{-6} cm (Kuo and Lauffenburger, 1993), the conversion factor was 8.3×10^{-16} mol-cm^2 molecule^{-1} L^{-1}.

RESULTS

Characterization of surfaces containing immobilized peptides

Derivatization of glycophase glass with linear RGD at an estimated surface density of 12 pmol/cm^2 (7.22×10^{12} molecules/cm^2) produced noticeable differences in the XPS spectra. The nitrogen content increased from 0.78% on glycophase glass to 1.56% on the RGD-derivatized glycophase glass. Nitrogen on glycophase glass represents adventitious nitrogen. As each RGD peptide contained eight nitrogen atoms and the silicon atomic percent of glycophase glass was 16, the calculated surface coverage (N/Si ratio) with peptide, after subtracting adventitious nitrogen, was 0.60%. This compares favorably with values (0.60–1.8%) calculated using the estimated peptide number density and a silanol density of 4×10^{14} to 12×10^{14} cm^{-2} (Pleuddemann, 1991). Further evidence for the presence of peptide was an increase in the ratio of carbonyl (288–289 eV) to total carbon from 0.065 on glycophase glass to 0.138 on RGD-derivatized glycophase glass.

Much smaller changes in the XPS spectra were observed at an estimated surface density of 3.8 pmol/cm^2 (2.29×10^{12} molecules/cm^2) The nitrogen content was 0.39% on glycophase glass, 0.51% on RGD-derivatized glycophase glass, and 0.62% on glycophase glass derivatized with cyclic RGD. The peptide surface coverage, based upon the N/Si ratio, is between 0.10 and 0.16%, which is at the lower end of values calculated from the estimated peptide density (0.1–0.57%). The carbonyl to total carbon ratio was 0.038 on glycophase glass, 0.040 on RGD-derivatized glycophase glass, and 0.046 on glycophase glass derivatized with cyclic RGD. Sulfur present in the cyclic RGD was not detected. These results are consistent with the low density of immobilized RGD peptides on glycophase glass.

Further support for the presence of immobilized peptides is provided by BAEC spreading after 4 h of attachment in serum-free medium. At an estimated peptide density of 2.45×10^{12} molecules/cm^2, projected areas were 1160 ± 719 μm^2 and 1070 ± 629 μm^2 for immobilized cyclic RGD and linear RGD, respectively. The projected area on untreated glycophase glass was 221 ± 99 μm^2. For a Fn density of 2.02×10^{11} on glass, the projected area was 2410 ± 1240 μm^2.

Cell detachment from immobilized RGD and adsorbed Fn

The strength of adhesion was measured for BAECs attached for 15 min to surfaces containing immobilized RGD. Fig. 4 shows the relation between applied shear stress and cell detachment from cyclic and linear RGD surfaces at densities of 2.3×10^9 molecules/cm^2. For each condition, data from several experiments were pooled and fit to the log-normal distribution. As shown by the curves in Fig. 4, data were well fit by a log-normal distribution. The critical shear

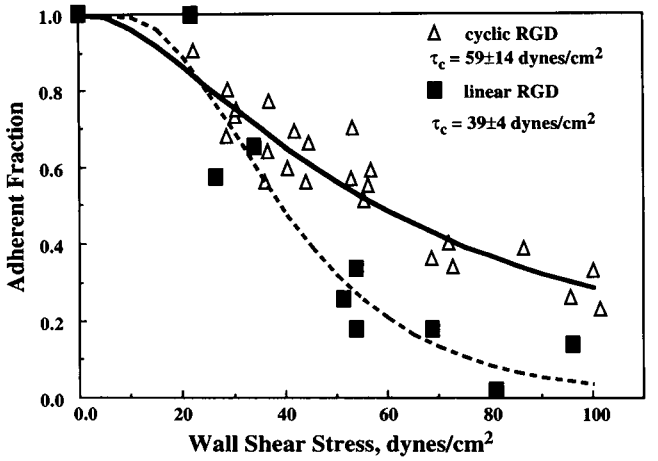

FIGURE 4 Fraction adherent versus wall shear stress (τ_w) for BAECs adherent to surfaces containing immobilized linear and cyclic RGD peptides at a density of 2.3×10^9 molecules/cm^2. The critical wall shear stresses were determined by nonlinear regression of the cumulative log-normal distribution function to pooled data. Best-fit curves are shown for BAECs adherent to immobilized linear RGD (- - -) and cyclic RGD (——).

stresses were 59 ± 13 dyne cm^{-2} (n = 3) for cyclic RGD and 39 ± 4 dyne cm^{-2} (n = 2) for linear RGD, respectively ($p < 0.01$).

Detachment of endothelial cells with trypsin instead of EGTA reduced the strength of adhesion to immobilized RGD. At a cyclic RGD surface density of 2.3×10^9 molecules/cm^2, cells removed with trypsin had a critical shear stress of 37 ± 5 dyne cm^{-2} whereas cells removed with EGTA had a critical shear stress of 59 ± 13 dyne cm^{-2}. Trypsin did not affect the adhesion strength of cells attached to adsorbed Fn. As the Vn receptor ($\alpha_v\beta_3$) is more sensitive to trypsin (Preissner et al., 1988) than the Fn receptor ($\alpha_5\beta_1$) (Akiyama and Yamada, 1985), these results are consistent with the specificity of linear and cyclic RGD peptides for the Vn receptor (Massia and Hubbell, 1991; Pierschbacher and Ruoslahti, 1987). All subsequent experiments were performed using EGTA to detach cells.

Critical shear stresses increased with increasing ligand density for BAECs attached to linear and cyclic RGD (Fig. 5 *A*) and adsorbed Fn (Fig. 5 *B*). β-Mercaptoethanol was not used to block unreacted tresyl chloride on the surface to prevent inactivation of cyclic RGD. As a result, considerable adhesion occurred on activated glycophase glass in the absence of RGD peptides (τ_c = 31 ± 6 dyne cm^{-2}). To account for this nonspecific adhesion, the critical shear stress was measured with immobilized RAD peptides at the same densities used with RGD peptides. The critical shear stresses for immobilized RAD surfaces did not vary with ligand density (Fig. 5 *A*).

Fig. 5 *B* shows critical shear stresses for BAEC detachment from Fn absorbed to glycophase and plain glass. Glycophase glass, which had not reacted with tresyl chloride, supported negligible adhesion, with τ_c equal to 2.0 ± 0.2 dyne cm^{-2}. The critical shear stress on glass without

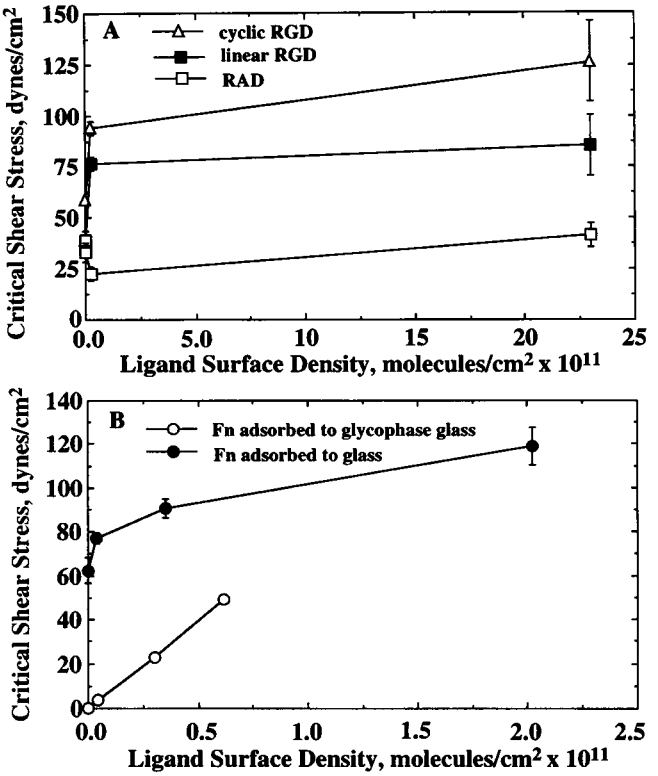

FIGURE 5 Critical shear stress needed to detach BAECs from surfaces containing immobilized peptides (*A*) or adsorbed Fn (*B*). Error bars represent standard deviations for best-fit values of the critical shear stresses.

adsorbed Fn was 62.5 ± 11.5 dyne cm^{-2}. After subtracting the nonspecific critical shear stress from the glass surface, the critical shear stresses for BAECs adherent to Fn adsorbed to the two different surfaces were less than the values for BAECs attached to immobilized RGD peptides.

Cell contact area measured by TIRFM

The strength of adhesion increased nonlinearly with the ligand density (Fig. 5). This nonlinear behavior could be due, in part, to variations in the contact area with ligand density. For each treatment, between 5 and 15 cells were examined by TIRFM and the contact area determined as a function of separation distance. Fig. 6 shows representative TIRFM images (Fig. 6, *A* and *C*) and separation contours (Fig. 6, *B* and *D*) for BAECs attached to immobilized cyclic RGD at ligand densities of 2.3×10^9 molecules/cm^2 and 2.3×10^{12} molecules/cm^2. At the lowest ligand density, the cell contour was very irregular, with many small projections (Fig. 6 *B*). At higher ligand densities (Fig. 6 *D*), the contour became smoother. Surfaces containing immobilized RGD and adsorbed Fn exhibited similar shapes.

From TIRFM images, the cumulative contact area was determined as a function of separation distance (Fig. 7). The contact area increased with increasing ligand surface density. For a given separation distance and ligand density, contact areas were slightly larger for BAECs attached to

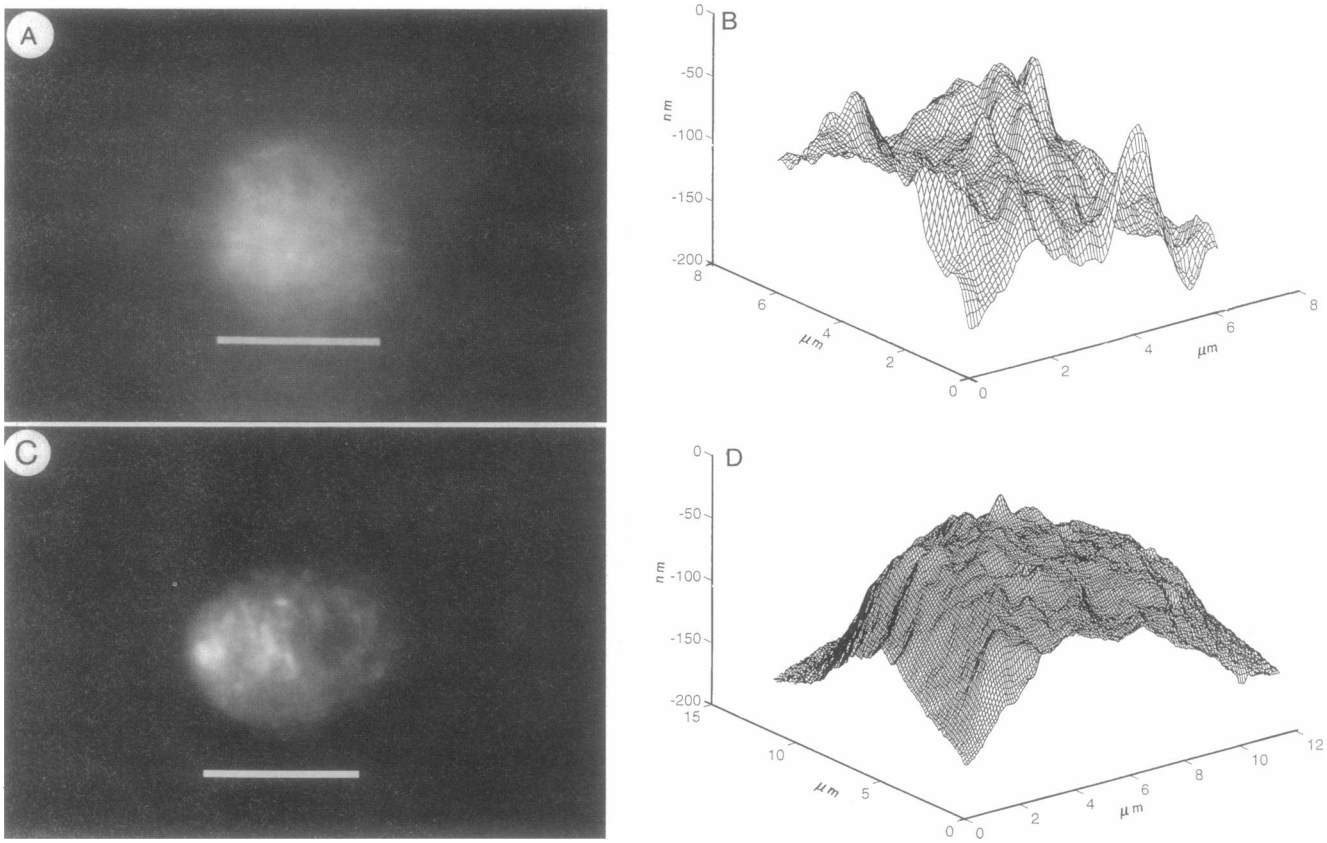

FIGURE 6 TIRFM images (*A* and *C*) and separation distance contours (*B* and *D*) of cells adherent to immobilized cyclic RGD at densities of 2.3×10^9 molecules/cm^2 and 2.3×10^{12} molecules/cm^2, respectively. Bar in *A* equals 10 μm.

immobilized linear RGD than to cyclic RGD. The contact areas were significantly larger on surfaces with adsorbed Fn than on surfaces with immobilized RGD peptides. To use these data in the calculation of receptor-ligand dissociation constants, the cumulative contact area for each ligand was fit to a cubic polynomial. Correlation coefficients were greater than 0.99.

Determination of receptor-ligand dissociation constants

Values of K_{Do}, κ, and N_{Ro} for immobilized RGD peptides or adsorbed Fn were determined by nonlinear regression of data to the uniform stress and peeling models as described in Materials and Methods. Listed in Table 2 are best-fit values of K_{Do}, κ, and N_{Ro} as well as sums of squares of the residuals. Best-fit curves are shown in Fig. 8. For immobilized peptides the uniform stress model provided a slightly better fit than the peeling model. The difference between the models was more pronounced with immobilized linear RGD than cyclic RGD. For Fn on glass and glycophase glass, the peeling model produced a substantially better fit, although the uniform stress model provided a better fit of data for cell adhesion at low densities of Fn adsorbed to glycophase glass.

Statistically significant differences in the affinity constants for immobilized linear and cyclic RGD were found with both models (Table 2). The affinity of cyclic RGD for its receptor was approximately two orders of magnitude greater than the value for linear RGD. For the peeling model, the affinity constants of cells attached to Fn adsorbed on glass or glycophase glass were not different than the affinity constant for linear RGD. With the uniform stress model, the affinity of Fn adsorbed on glass for its receptor was greater than the affinity of Fn adsorbed on glycophase glass and less than the affinity of linear RGD for its receptor. This difference in affinity between immobilized RGD and adsorbed Fn obtained with the uniform stress model is consistent with the smaller contact areas (Fig. 7) and greater net detachment forces (Fig. 8) of cells attached to immobilized RGD peptides.

In solution, linear and cyclic RGD bind to the Vn receptor ($\alpha_v\beta_3$) with K_{Do} equal to 10^{-3} M and 10^{-4} M, respectively (Pierschbacher and Ruoslahti, 1987). In solution, the affinity of Fn for its receptor ($\alpha_5\beta_1$) is approximately 10^{-6} M (Akiyama and Yamada, 1985) and the affinity of Vn for its receptor ($\alpha_V\beta_3$) is 0.2×10^{-6} M (Preissner et al., 1988). For the uniform stress model, the affinity constants for immobilized Fn are not statistically different than values obtained for Fn in solution (Akiyama and Yamada, 1985)

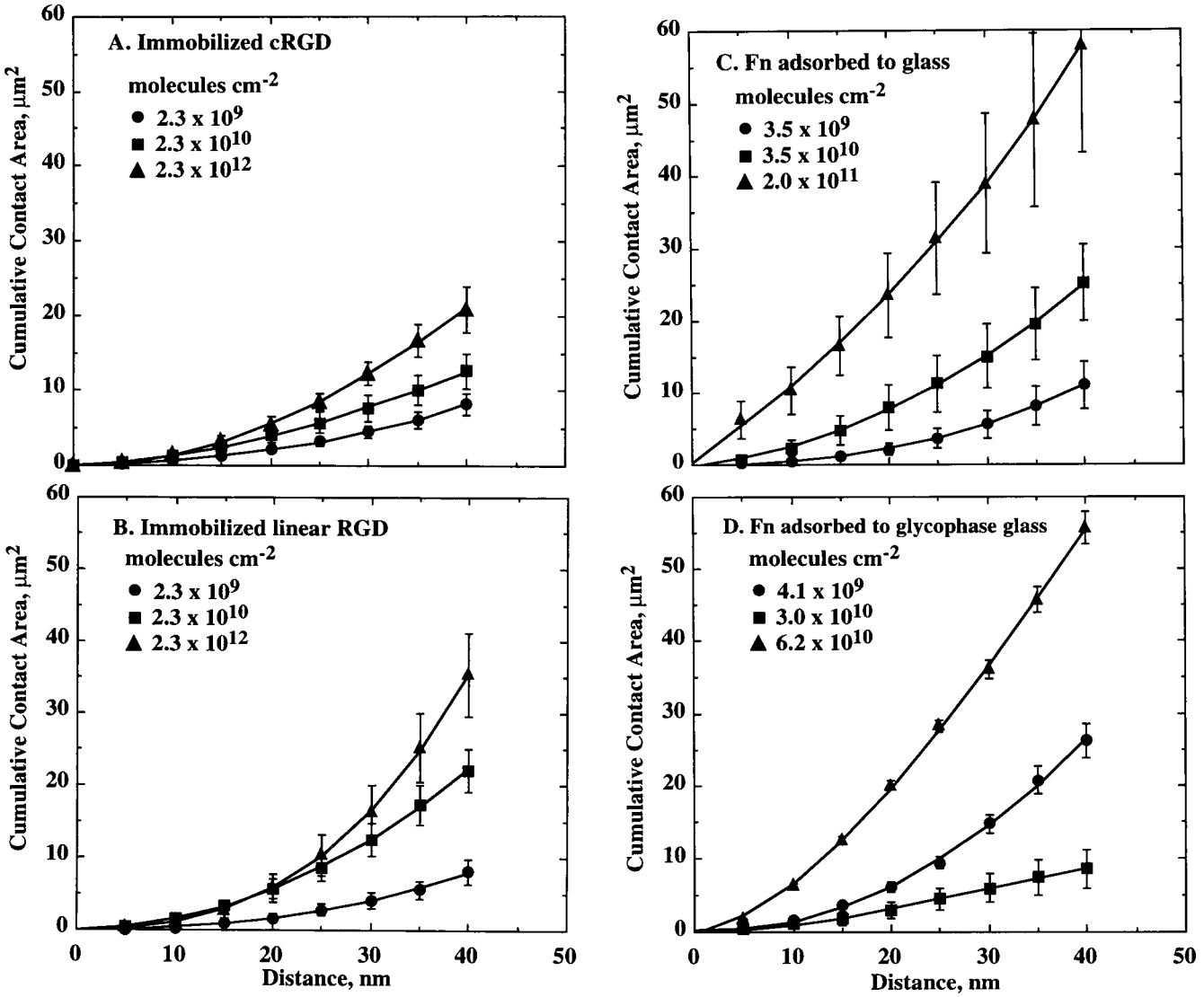

FIGURE 7 Cumulative contact area as a function of membrane-substrate separation distance. Error bars represent standard error of the mean.

whereas the affinity constants obtained with the peeling model are much smaller than values measured in solution. The affinity constants for immobilized RGD peptides for the $\alpha_V\beta_3$ integrin are substantially smaller than the values for peptides in solution (Pierschbacher and Ruoslahti, 1987). For cells attached to immobilized RGD peptides, the fitted value for K_{Do} between the receptor and ligand must be small enough so that a sufficient number of bonds are present to balance the hydrodynamic force. With or without the constraints imposed upon κ and N_{Ro}, no set of initial guesses for the nonlinear regression produced a larger value of K_{Do}.

The estimated affinity constant is affected by the accuracy of values for the RGD peptide and receptor densities. Higher receptor or ligand densities than those used in the calculations would require larger values of K_{Do}. With adsorbed Fn, radiolabeling measures the total density of ligand on the surface, not the active fraction. Very likely, only a fraction of adsorbed Fn is active (Massia and Hubbell, 1991). For the RGD densities studied, the amount of soluble RGD equals the amount of immobilized RGD (Massia and Hubbell, 1990). Thus, the surface density of RGD peptides was limited by the amount of peptide supplied for the immobilization reaction. A higher receptor density and a lower affinity constant would permit a sufficient number of bonds to form at low ligand densities but would produce too many bonds at the higher ligand densities.

Determination of force per bond

Once the receptor-ligand dissociation constants were determined, the bond density was calculated and the force per bond determined. For the uniform stress model, the force per bond was calculated from a modified form of Eq. 15 that

TABLE 2 Dissociation constants of immobilized RGD peptides and adsorbed fibronectin

Ligand	K_{D_o} (M)	κ	$N_{R_o} \times 10^{10}$	Sums of squares
Peeling model				
Cyclic RGD	$2.8 \pm 12.4 \times 10^{-13}$		2.8 ± 2.3	3.99×10^{-8}
Linear RGD	$4.6 \pm 20.0 \times 10^{-10}$*	1.0 ± 1.5		3.16×10^{-8}
Fn on glass	$1.6 \pm 8.7 \times 10^{-9}$		0.78 ± 0.98	5.01×10^{-8}
Fn on glycophase	$5.0 \pm 0.01 \times 10^{-10}$			2.99×10^{-8}
Uniform stress model				
Cyclic RGD	$1.5 \pm 1.3 \times 10^{-12}$		0.500 ± 0.001	3.54×10^{-8}
Linear RGD	$2.8 \pm 7.0 \times 10^{-10}$#	1.2 ± 0.9		9.03×10^{-9}
Fn on glass	$5.1 \pm 67.7 \times 10^{-6}$§		0.501 ± 0.001	2.42×10^{-7}
Fn on glycophase	$1.3 \pm 19.4 \times 10^{-7}$			8.51×10^{-8}

*$0.002<p<0.005$.
#$0.001<p<0.005$.
§$0.025<p<0.05$.

accounts for nonspecific adhesion (Kuo and Lauffenburger, 1993):

$$F_T = F_{NS} + N_{LR} f_b A_c, \quad (20)$$

where F_{NS} is the nonspecific force of adhesion measured in the absence of ligand. For the peeling model, A_c was replaced with A_s (Eq. 18). Equation 20 indicates a linear relation between the total force on the cell and the number of bonds (bond density times stressed area). The bond density was found with Eq. 6 using best-fit values of K_{Do}, κ, and N_{Ro} for the peeling and uniform stress models. As K_{Do} from the peeling model did not differ for linear RGD and Fn adsorbed to glass and glycophase glass, these data were pooled and fit.

Summarized in Table 3 are the average bond forces for the uniform stress and peeling models along with values of r^2 and the statistical significance of the calculated bond force. For the peeling model, all of the data yielded good linear fits (Fig. 9 *A*). The force per bond for cyclic RGD-$\alpha_V\beta_3$ binding was greater than the value for linear RGD-$\alpha_V\beta_3$ binding or Fn-$\alpha_5\beta_1$ binding. For the uniform stress model (Fig. 9, *B* and *C*), good fits were obtained with immobilized RGD peptides, but the force per bond for adsorbed Fn was not significantly different from zero. The order of the bond forces was cyclic RGD > linear RGD > Fn adsorbed to glycophase glass ≈ Fn adsorbed to glass. The bond forces are positively correlated with the affinity constants.

The bond forces for the peeling model were 24–93% of the values obtained with the peeling model. The peeling model predicted that fewer bonds were stressed, yielding larger bond forces than the uniform stress model. The linearity between net force and number of bonds and the nonzero values for the force per bond observed with the peeling and uniform stress models suggests that both models adequately represent the detachment process.

DISCUSSION

Previously, the role of receptor-ligand affinity upon the strength of adhesion had not been examined with cells. Theoretical models indicate a logarithmic relationship between the force per bond and the dissociation constant (Bell, 1978; Dembo et al., 1988; Evans, 1985). These models have only been tested using a model cell system consisting of antibodies immobilized to polystyrene microspheres (Kuo and Lauffenburger, 1993). In the current study, adsorbed Fn and RGD peptides covalently immobilized to glycophase glass surfaces were used to assess the effect of ligand conformation and accessibility on the strength of endothelial cell adhesion. Results of this study indicate that 1) BAECs are more adherent on immobilized cyclic RGD peptide than linear RGD or adsorbed Fn, 2) increased adhesion is due to a greater affinity between cyclic RGD and its receptor, and 3) the affinity of RGD peptides and adsorbed Fn for their receptors is increased after immobilization.

An indirect approach was used to determine the receptor-ligand dissociation constant and the bond force for immobilized ligand. The analysis required calculation of the net force on the cells, the contact area between the cell and the surface, the receptor density, and the number of bonds formed between immobilized molecules and their receptors. The net hydrodynamic force acting on cells is sensitive to cell shape (Olivier and Truskey, 1993). To account for cell shape, the net hydrodynamic force on the cells was determined using two-dimensional models of spreading cells. The duration of the experiment was limited to 15 min to minimize cellular synthesis of Fn, remodeling of adsorbed proteins (Grinnell, 1986), or cell deformation (Truskey and Proulx, 1993).

The adhesive contact area depended upon the amount of cell area at a given distance from the surface as well as the density and rigidity of receptor-ligand bonds. The definition of the contact area was based upon the distance over which bonds could form (Bell, 1988; Ward and Hammer, 1993). Theoretical calculations showed that critical separation distance was larger for higher affinity interactions, higher ligand densities, and less rigid bonds (Fig. 2). TIRFM was used to quantitatively measure cell/substrate separation distances (Burmeister et al., 1994; Truskey et al., 1992). The amount of cell area at a given distance from the surface increased as the ligand density increased and was greater for

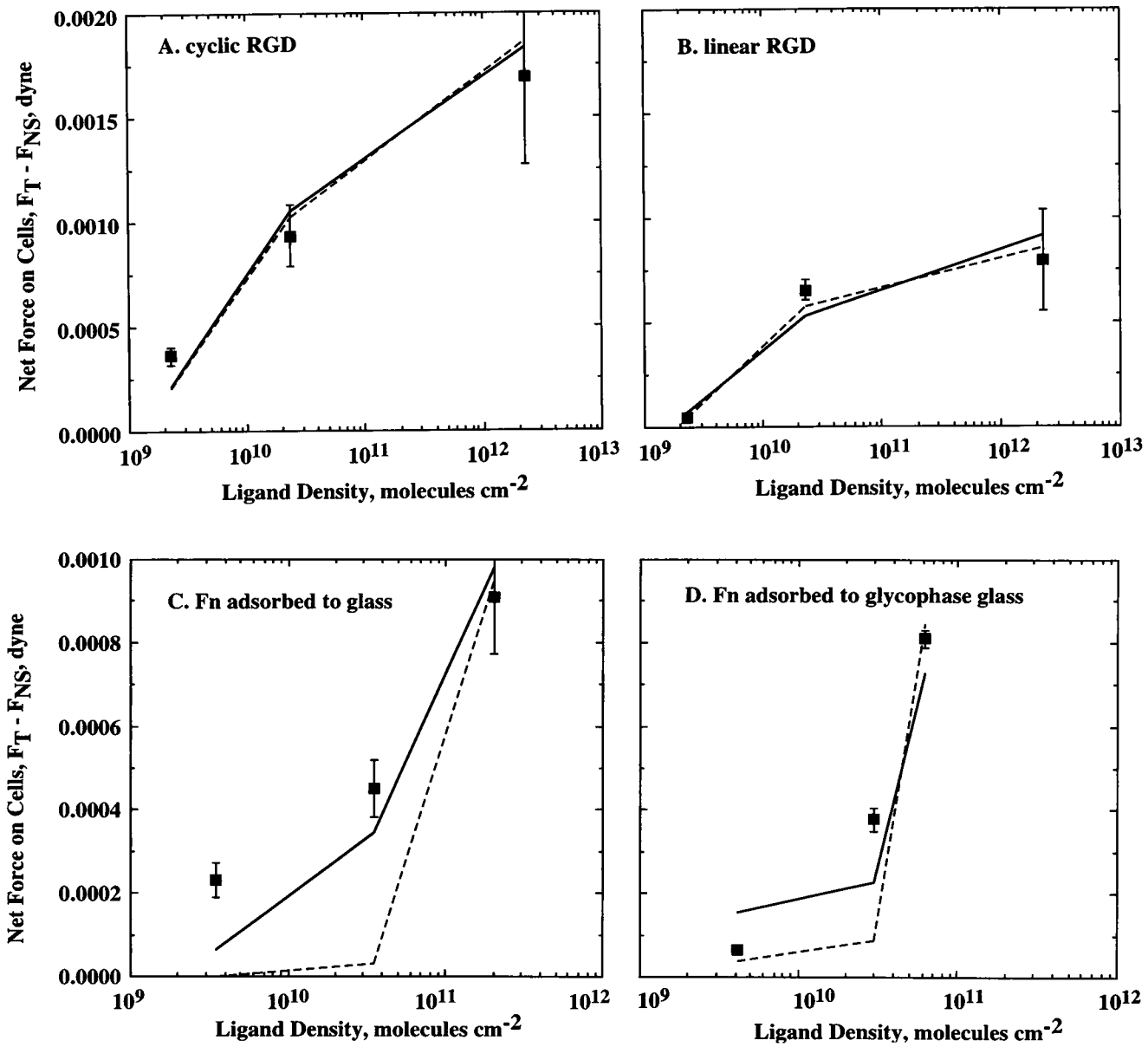

FIGURE 8 Best fit of uniform stress (dashed curves) and peeling (solid curves) models to net hydrodynamic force on cells as a function of ligand density. Net force represents the difference between total force and force due to nonspecific interactions in the absence of ligand. Best-fit values of K_{Do}, κ, and N_{Ro} are listed in Table 2.

cells attached to surfaces with adsorbed Fn than for cells attached to surfaces with covalently immobilized RGD peptides (Fig. 7). The larger contact area for the lower affinity Fn-integrin interactions suggests that the initial formation of contact area is not dependent upon receptor-ligand bond strength.

As the mechanical properties of endothelial cells are unknown, two limiting models of the bond stress distribution were considered: the uniform stress model and the peeling model. Both models gave very similar fits to the data for cells attached to immobilized RGD peptides, although the peeling model provided better fits to the data for cells attached to adsorbed Fn (Fig. 8). Furthermore, the relation between force on the cell and number of bonds was linear for both the peeling and uniform stress models. Verification that cells detached by peeling will require examination of membrane movement or receptor movement by TIRFM or other optical techniques. Further support for the results of the current analysis can be provided by direct measurement of the bond force using atomic force microscopy (Florin et al., 1994) or the newly developed biointerface probe (Evans et al., 1995).

A surprising result of this study is the increased affinity of immobilized RGD peptides and adsorbed Fn for their respective integrin receptors. Using a large range of initial guesses we failed to find a best-fit parameter set with values for K_{Do}

TABLE 3 Average force per bond

Ligand	Uniform stress model		Peeling model	
	F_b (μdyne)	r^2	F_b (μdyne)	r^2
Cyclic RGD	14.8 ± 2.0	0.964 ($0.01 < p < 0.02$)	15.9 ± 2.6	0.950 ($0.02 < p < 0.05$)
Linear RGD	11.6 ± 1.0	0.987 ($0.01 < p < 0.02$)		
Fn on glass	2.3 ± 0.8	0.810 ($0.05 < p < 0.10$)	9.7 ± 0.9	0.933 ($p < 0.0002$)
Fn on glycophase	4.4 ± 1.2	0.867 ($0.05 < p < 0.10$)		

similar to those for cell binding to RGD peptides in solution. Due to the stoichiometric addition of peptide to the surface for immobilization, uncertainties in the density of immobilized RGD could not produce lower values of K_{Do}. The increased affinity of the peptides may result from further constraints on the mobility of the peptide. The higher affinity of immobilized RGD peptides relative to adsorbed Fn is consistent with the observation that fibroblasts spread with densities of immobilized RGD peptides 30–110 times less than the density of adsorbed Fn (Massia and Hubbell, 1991).

Based upon results with the peeling model, the affinity between Fn and the integrin $\alpha_5\beta_1$ increased upon adsorption. Furthermore, not all of the adsorbed Fn may be functionally active. Conformational changes to the Fn cell-binding domain occur upon adsorption (Iuliano et al., 1993; Narasimhan et al., 1988). Upon adsorption, the RGD domain becomes more solvent accessible, thereby increasing the likelihood of binding. The polar environment on the surface appears to affect the extent to which the RGD binding domain is solvent accessible (Iuliano et al., 1993). Furthermore, when Fn adsorbs, a large fraction of the protein is not in a suitable conformation for binding to its integrin receptor (Massia and Hubbell, 1991), and a small fraction of adsorbed Fn exhibits increased affinity for its receptor.

Short RGD peptides and adsorbed Fn bound to integrins yielded similar spring constants of approximately 1 dyne cm^{-1}, which suggests that the spring may functionally reside with either the integrin molecule or the cytoskeleton. Erickson (1994) argues that Fn is quite flexible and can extend as much as 160 nm. When adsorbed to a surface, however, Fn may make multiple contacts with the surface and each segment may extend a shorter distance.

At ligand densities greater than the receptor density, receptors may accumulate in the contact region as a result of interactions with the cytoskeleton (Gingell and Owens, 1992; Ward and Hammer, 1993). Receptor accumulation will further increase the bond density. A model of receptor accumulation based upon equilibrium binding of receptor-bound integrin to the cytoskeleton protein talin has recently been developed (Ward and Hammer, 1993). For the highest ligand density used in this study, 2.3×10^{12}, a focal contact area of 5.2×10^{-8} cm^2, and physiological values for talin density, this model predicts that receptor density in the contact area is increased 25–75% above the density in the absence of clustering. This small increase of receptor density lies within the error of the data. Receptor accumulation could be significant for higher ligand densities or longer incubation times.

Evans and colleagues (1991) measured forces between 1 and 2 μdyne to break individual attachments between red cells produced by either antibodies to the integral membrane proteins glycophorin and blood type A antigens or a lectin that binds to glycolipids. The bond forces were explained by extraction of the receptor through the cell membrane. Except for the analysis of adsorbed Fn with the uniform stress model, bond forces were considerably larger than those measured for ligand interactions with the red cell membrane receptors. This different behavior could be due to integrin interaction with the endothelial cell cytoskeleton. Integrins form interactions with the cytoskeleton within 15 min of binding to their ligand (Lotz et al., 1989; Plopper and Ingber, 1993; Wang et al., 1993). Further support for integrin engagement with the cytoskeleton is provided by recent studies using the biointerface probe (Evans et al., 1995) and laser tweezers (Schmidt et al., 1993). Binding of cell membrane receptors to ligand triggers cytoskeleton retraction. As a result, forces between 10 and 15 μdyne are required to separate the receptor and ligand (Evans et al., 1995).

The range of bond forces observed in this study is similar to that measured for several different receptor-ligand systems. Kuo and Lauffenburger (1993) studied the strength of adhesion between antibodies immobilized to beads and adsorbed antigens. They found bond forces between 1.1 μdyne for K_{D_o} equal to 10^{-5} M and 7.4 μdyne for K_{Do} equal to 10^{-9} M. The force to break an avidin interaction with biotin measured by atomic force microscopy is 16 ± 2 μdyne/bond (Florin et al., 1994). The bond force was reduced for desthiobiotin, which exhibits a lower affinity for avidin. Chu et al. (1994) examined the strength of adhesion of rat basophilic cells to immobilized dinitrophenol via IgE and measured bond force between 2 and 4 μdyne, although the effect of affinity was not studied.

Results of this study suggest that strong endothelial cell adhesion can be obtained using immobilized cyclic RGD. For the same surface and bond density, the force per bond is approximately two times greater for immobilized cyclic RGD than adsorbed Fn. Consequently, adherent endothelial cells should resist a proportionately larger shear stress when attached to cyclic RGD than Fn. Although the effect of affinity is modest, we speculate that this difference in adhesion strength should be sufficient to promote stronger endothelial cell adhesion on vascular grafts under physiological conditions.

Helpful discussions with D. Needham and W. M. Reichert at Duke University are gratefully appreciated. We thank K. Barber for the analysis of

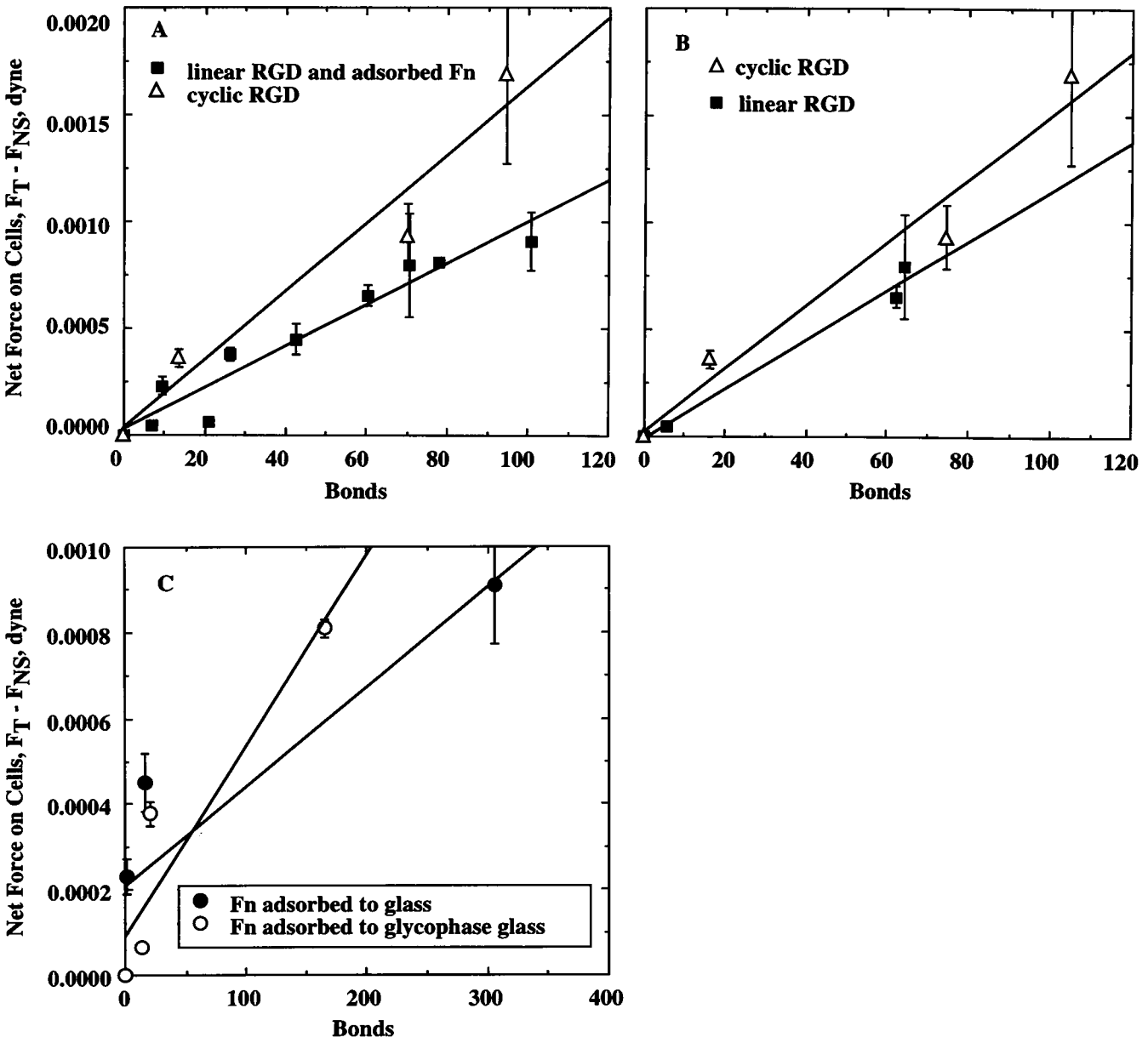

FIGURE 9 Net hydrodynamic force versus number of ligand-receptor bonds in contact area for the peeling model (*A*) and uniform stress (*B* and *C*) models. As K_{Do} from the peeling model was not different for linear RGD and adsorbed Fn, these data were fit together to obtain a single bond force (*A*). The bond density was calculated from the best-fit values of K_{Do}, κ, and N_{Ro} listed in Table 2. The number of bonds equals the product of the bond density times the contact area. Error bars are due to variations in contact area. The force per bond was calculated from the slope of the line and values are listed in Table 3.

the forces on the cells. This paper is dedicated to the memory of Claire Yung-Ming Truskey.

This work was supported by National Institutes of Health grant HL44972 and a grant-in-aid from the American Heart Association (93012390).

APPENDIX

Calculation of critical tension

Limiting expressions for the critical tension exist for the limit of low (Dembo et al., 1988) and high ligand density (Ward et al., 1995). For intermediate cases, the critical tension was obtained by numerical solution of the equations of membrane mechanics (Ward et al., 1995). In this appendix, we use an equilibrium thermodynamics approach to derive an analytical expression for the critical tension valid for all ligand densities (Dembo, 1994; Torney et al., 1986). Consider a cell in contact with a surface over a region A_c. Equilibrium is assumed between receptors on the cell and ligand on the surface. Bonds are under stress resulting from the application of an external force on the cell. The total Gibbs free energy for the system is a function of the contact area A_c, separation distance $\Delta(x,y)$, ligand N_L, receptor N_R, and bond N_{LR}, densities, and membrane tension T_m:

$$G(A_c, \Delta(x, y), N_{LR}) = G_o + G_{N_L} + G_{N_R} + G_{N_{LR}} + G_{T_m}, \quad \text{(A1)}$$

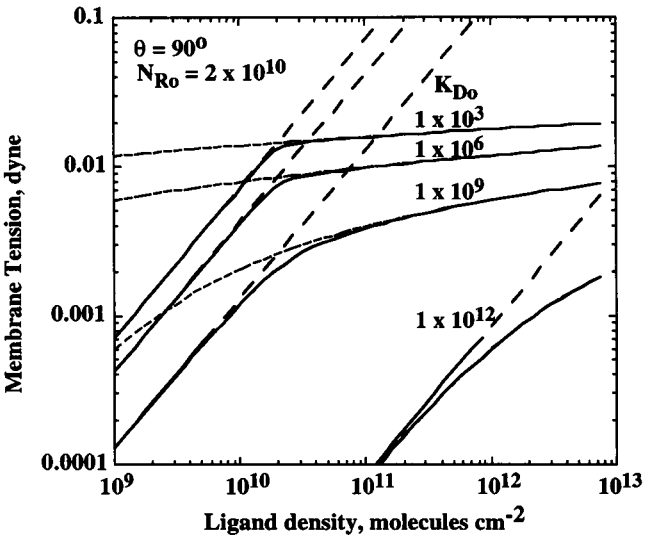

FIGURE A1 Membrane tension as a function of ligand density and unstressed equilibrium constant (K_{Do}) for a critical angle (θ) of 90° and a receptor density of 2×10^{10} molecules cm^{-2}. Solid curves represent Eq. A8 and the dashed curves represent limiting expressions valid when $N_{Ro} \ll N_{Lo}$, Eq. A10 (– – –), and $N_{Lo} \ll N_{Ro}$, Eq. A12 (- - -)

where G_o is the Gibbs free energy in the reference state, G_{NL} is the Gibbs free energy of the ligand, G_{NR} is the Gibbs free energy of the receptor, G_{NLR} is the Gibbs free energy of the receptor-ligand complex, and G_{Tm} is the Gibbs free energy arising from deforming the membrane. Nonspecific interactions between the cell and substrate have been neglected. Expressions for the individual Gibbs free energies are (Dembo, 1994)

$$G_{N_L} = \mu_L^o(A_{sub} - A_c)N_{L_o} + kT(A_{sub} - A_c)N_{L_o}\ln(N_{L_o}) + \mu_L^o A_c(N_{L_o} - N_{LR}) + kTA_c(N_{L_o} - N_{LR})\ln \cdot (N_{L_o} - N_{LR}) \quad (A2)$$

$$G_{N_R} = \mu_R^o(A_{mem} - A_c)N_{R_o} + kT(A_{mem} - A_c)N_{R_o}\ln(N_{R_o}) + \mu_R^o A_c(N_{R_o} - N_{LR}) + kTA_c(N_{R_o} - N_{LR})\ln \cdot (N_{R_o} - N_{LR}) \quad (A3)$$

$$G_{N_{LR}} = \mu_{LR}^o A_c N_{LR} + A_c N_{LR} kT\ln(N_{LR}) + A_c N_{LR} 0.5\kappa(\Delta(x, y) - \Delta_o)^2 \quad (A4)$$

$$G_{T_m} = [A_c(1 + \cos\theta) - A_{mem}]T_m, \quad (A5)$$

where μ_L^o, μ_R^o, and μ_{LR}^o are the chemical potential of the ligand, receptor, and receptor-ligand complex in the reference state, A_{mem} is the surface area of the cell membrane, and A_{sub} is the substrate surface area. The equilibrium state is found by taking the derivative of the Gibbs free energy with respect to each of the three system variables ($\Delta(x,y)$, N_{LR}, and A_c) and setting the derivatives to zero. For

$$\frac{\partial G(A_c, \Delta(x, y), N_{LR})}{\partial N_{LR}} = 0,$$

equilibrium of stressed bonds requires that

$$\frac{(N_{R_o} - N_{LR})(N_{L_o} - N_{LR})}{N_{LR}} = K_{D_o}\exp\left[\frac{0.5\kappa(\Delta(x, y) - \Delta_o)^2}{kT}\right], \quad (A6)$$

where the equilibrium constant for unstressed bonds K_{Do} equals

$$\exp\left[\frac{\mu_{LR}^o - \mu_R^o - \mu_L^o}{kT} - 1\right].$$

At equilibrium, the separation distance Y is found by setting

$$\frac{\partial G(A_c, \Delta(x, y), N_{LR})}{\partial \Delta(x, y)}$$

equal to zero. This yields the result that $\Delta(x,y) = \Delta_o$. The third equilibrium relation is found by setting

$$\frac{\partial G(A_c, \Delta(x, y), N_{LR})}{\partial A_c}$$

equal to zero. After rearrangement and setting $\Delta(x,y) = \Delta_o$, we have

$$(1 + \cos\theta)T_{crit} = (\mu_R + \mu_L^o - \mu_{LR}^0)N_{LR} + kTN_{LR}\ln\left[\frac{(N_{R_o} - N_{LR})(N_{L_o} - N_{LR})}{N_{LR}}\right] + kTN_{R_o}\ln\left[\frac{N_{R_o}}{(N_{R_o} - N_{LR})}\right] + kTN_{L_o}\ln\left[\frac{N_{L_o}}{(N_{L_o} - N_{LR})}\right]. \quad (A7)$$

Using Eq. A6, this result can be simplified to the following expression for the critical tension:

$$T_{crit} = \frac{kT}{(1 + \cos\theta)}\left\{-N_{LR} + N_{R_o}\ln\left[\frac{N_{R_o}}{(N_{R_o} - N_{LR})}\right] + N_{L_o}\ln\left[\frac{N_{L_o}}{(N_{L_o} - N_{LR})}\right]\right\} \quad (A8)$$

Solution of Eq. A6 yields a quadratic expression for N_{LR}, which can be substituted into Eq. A8.

Limiting cases of Eq. A8 can be derived. For $N_{Ro} \ll N_{Lo}$,

$$\ln\left[\frac{(N_{L_o} - N_{LR})}{N_{L_o}}\right] \approx -\frac{N_{LR}}{N_{L_o}},$$

and Eq. A8 reduces to

$$(1 + \cos\theta)T_m = -kTN_{R_o}\ln\left[1 - \frac{N_{LR}}{N_{R_o}}\right]. \quad (A9)$$

As $N_{Ro} \ll N_{Lo}$ and $Y = L$, the bond density simplifies to

$$N_{LR} = \frac{N_{R_o}N_{L_o}}{N_{L_o} + K_{D_o}}. \quad (A10)$$

Substituting for N_{LR} in Eq. A9 with Eq. A10 and rearranging yields

$$(1 + \cos\theta)T_m = kTN_{R_o}\ln\left[1 + \frac{N_{L_o}}{K_{D_o}}\right], \quad (A11)$$

which is identical to the result derived by Dembo et al. (1988). In a similar

fashion, if $N_{Lo} \ll N_{Ro}$, the following results:

$$(1 + \cos\theta)T_m = kTN_{L_o}\ln\left[1 + \frac{N_{R_o}}{K_{D_o}}\right] \qquad \text{(A12)}$$

Eqs. A8, A11, and A12 are compared in Fig. A1. Results are similar to those presented by Ward et al. (1995).

REFERENCES

Akiyama, S. K., and K. M. Yamada. 1985. The interaction of plasma fibronectin with fibroblastic cells in suspension. *J. Biol. Chem.*, 60: 4492–4500.

Alon, R., D. A. Hammer, and T. A. Springer. 1995. Lifetime of the P-selectin-carbohydrate bond and its response to tensile force in hydrodynamic flow. *Nature*. 374:539–542.

Batchelor, G. K. 1967. An Introduction to Fluid Dynamics. Cambridge University Press, Cambridge, UK.

Bates, D. M., and D. G. Watts. 1988. Nonlinear Regression Analysis and Its Applications. John Wiley and Sons, New York.

Bell, G. I. 1978. Models for the specific adhesion of cells to cells. *Science*. 200:618–627.

Bell, G. I. 1988. Models of cell adhesion involving specific binding. *In* Cell-Cell Adhesion. P. Bongrand, editor. CRC Press, Boca Raton, FL. pp. 227–256.

Bird, R. B., W. E. Stewart, and E. N. Lightfoot. 1960. Transport Phenomena. John Wiley and Sons, New York.

Burmeister, J. S., G. A. Truskey, and W. M. Reichert. 1994. Quantitative analysis of variable-angle total internal reflection fluorescence microscopy (VA-TIRFM) of cell/substrate contacts. *J. Microscopy*. 173:39–51.

Chen, W. T., and S. J. Singer. 1982. Immunoelectron microscopic studies of the sites of cell-substratum and cell-cell contacts in cultured fibroblasts. *J. Cell Biol.* 95:205–222.

Conforti, G., A. Zanetti, S. Colella, M. Abbadini, P. C. Marchisio, R. Pytela, F. Giancotti, G. Tarone, L. R. Languino, and E. Dejana. 1989. Interaction of fibronectin with cultured human endothelial cells: characterization of the specific receptor. *Blood*. 6:1576–1585.

Craig, W. S., S. Cheng, D. G. Mullen, J. Blevitt, and M. D. Pierschbacher. 1995. Concept and progress in the development of RGD-containing peptide pharmaceuticals. *Biopolymers*. 37:157–175.

Dekker, A., T. Beugiling, A. Poot, J. Spijders, J. A. van Mourik, J. Feijen, A. Bantjes, and W. G. van Aken. 1993. The role of cellular fibronectin in the interaction of human endothelial cells with polymers. *Clin. Materials*. 13:101–107.

Dembo, M. 1994. On peeling an adherent cell from a surface. *Math. Questions Biol. Lect. Math. Life Sci.* 24:51–78.

Dembo, M., D. C. Torney, D. Saxman, and D. A. Hammer. 1988. The reaction-limited kinetics of membrane-to-surface adhesion and detachment. *Proc. R. Soc. Lond. B.* 234:55–83.

Denn, M. M. 1980. Process Fluid Mechanics. Prentice-Hall, Englewood Cliffs, NJ.

Erickson, H. P. 1994. Reversible unfolding of fibronectin type III and immunoglobulin domains provides the structural basis for stretch and elasticity of titin and fibronectin. *Proc. Natl. Acad. Sci. USA*. 91: 10114–10118.

Evans, E. 1985. Detailed mechanics of membrane-membrane adhesion and separation. I. Continuum of molecular cross-bridges. *Biophys. J.* 45: 175–183.

Evans, E., D. Berk, and A. Leung. 1991. Detachment of agglutinin-bonded red blood cells. I. Forces to rupture molecular-point attachments. *Biophys. J.* 59:838–848.

Evans, E., K. Ritchie, and R. Merkel. 1995. Sensitive force technique to probe molecular adhesion and structural linkages at biological interfaces. *Biophys. J.* 68:2580–2587.

Florin, E. L., V. T. Moy, and H. E. Gaub. 1994. Adhesion forces between individual ligand-receptor pairs. *Science*. 264:415–417.

Garrison, M. D., D. J. Iuliano, S. S. Saavedra, and W. M. Reichert. 1992. Post-adsorption changes in the emission maximum of acrylodan-labelled bovine serum albumin using TIRF. *J. Colloid Interface Sci.* 148:415–422.

Gingell, D., and N. Owens. 1992. How do cells sense and respond to adhesive contacts? diffusion-trapping of laterally mobile membrane proteins at maturing adhesions may initiate signals leading to local cytoskeletal assembly response and lamella formation. *J. Cell Sci.* 101:255–266.

Giroux, T. A., and S. L. Cooper. 1990. FTIR/ATR studies of human fibronectin adsorption onto plasma derivatized polystyrene. *J. Colloid Interface Sci.* 139:351–362.

Goldman, A. J., R. G. Cox, and H. Brenner. 1967a. Slow viscous motion of a sphere parallel to a plane wall. II. Couette flow. *Chem. Eng. Sci.* 22:653–660.

Goldman, A. J., R. G. Cox, and H. Brenner. 1967b. Slow viscous motion of a sphere parallel to a plane wall. I. Motion through a quiescent fluid. *Chem. Eng. Sci.* 22:637–651.

Grinnell, F. 1986. Focal adhesion sites and the removal of substratum-bond fibronectin. *J. Cell Biol.* 103:2697–2706.

Grinnell, F., and M. K. Feld. 1982. Fibronectin adsorption on hydrophilic and hydrophobic surfaces detected by antibody binding and analyzed during cell adhesion in serum-containing medium. *J. Biol. Chem.* 257: 4888–4893.

Hammer, D. A., and D. A. Lauffenburger. 1987. A dynamical model for receptor-mediated cell adhesion to surfaces. *Biophys. J.* 52:475–487.

Hyman, W. A. 1972. Shear flow over a protrusion from a plane wall: addendum. *J. Biomech.* 5:643.

Hynes, R. O. 1992. Integrins: versatility, modulation, and signaling in cell adhesion. *Cell*. 69:11–25.

Iuliano, D. J., S. S. Saavedra, and G. A. Truskey. 1993. Effect of the conformation and orientation of adsorbed fibronectin on endothelial cell spreading and the strength of adhesion. *J. Biomed. Materials Res.* 27:1103–1113.

Kuo, S. C., and D. A. Lauffenburger. 1993. Relationship between receptor/ligand binding affinity and adhesion strength. *Biophys. J.* 65:2191–2200.

Lotz, M. M., C. A. Burdsal, H. P. Erickson, and D. R. McClay. 1989. Cell adhesion to fibronectin and tenascin: quantitative measurements of initial binding and subsequent strengthening response. *J. Cell Biol.* 109: 1795–1805.

Massia, S. P., and J. A. Hubbell. 1990. Covalent surface immobilization of Arg-Gly-Asp- and Tyr-Lle-Gly-Ser-Arg-containing peptides to obtain well-defined cell-adhesive substrates. *Anal. Biochem.* 187:292–301.

Massia, S. P., and J. A. Hubbell. 1991. An RGD spacing of 440 nm is sufficient for integrin $\alpha_v\beta_3$-mediated fibroblast spreading and 140 nm for focal contact and stress fiber formation. *J. Cell Biol.* 114:1089–1100.

Massia, S. P., and J. A. Hubbell. 1992. Immobilized amines and basic amino acids as mimetic heparin-binding domains for cell surface proteoglycan-mediated adhesion. *J. Biol. Chem.* 267:10133–10141.

Narasimhan, C., C. S. Lai, A. Haas, and J. McCarthy. 1988. One free sulfhydryl group of plasma fibronectin becomes titratable upon binding of the protein to solid substrates. *Biochemistry*. 27:4970–4973.

Nicol, A., D. C. Gowda, and D. W. Urry. 1992. Cell adhesion and growth on synthetic elastomeric materials containing ARG-GLY-ASP-SER. *J. Biomed. Materials Res.* 26:393–413.

Olivier, L. A., and G. A. Truskey. 1993. A numerical analysis of forces exerted by laminar flow on spreading cells in a parallel plate flow chamber assay. *Biotechnol. Bioeng.* 42:963–973.

Pierschbacher, M. D., and E. Ruoslahti. 1987. Influence of stereochemistry of the sequence Arg-Gly-Asp-Xaa on binding specificity in cell adhesion. *J. Biol. Chem.* 262:17294–17298.

Pleuddemann, E. P. 1991. Silane Coupling Agents, 2nd ed. Plenum Press, New York.

Plopper, G., and D. E. Ingber. 1993. Rapid induction and isolation of focal adhesion complexes. *Biochem. Biophys. Res. Commun.* 193:571–578.

Preissner, K. T., E. Anders, J. Grulich-Henn, and G. Muller-Berghaus. 1988. Attachment of human endothelial cells is promoted by specific association with S protein (vitronectin) as well as with the ternary S protein-thrombin-antithrombin III complex. *Blood*. 71:1581–1589.

Reichert, W. M. 1989. Evanescent detection of adsorbed protein films: assessment of optical considerations for absorbance and fluorescence spectroscopy at the crystal/solution and polymer/solution interfaces. *Crit. Rev. Biocompat.* 5:173–205.

Reichert, W. M., and G. A. Truskey. 1990. Total internal reflection fluorescence microscopy (TIRF). I. Modeling of cell contact region fluorescence. *J. Cell Sci.* 96:219–230.

Ruoslahti, E., E. G. Hayman, M. D. Pierschbacher, and E. Engvall. 1988. Fibronectin: purification, immunochemical properties, and biological activities. *Methods Enzymol.* 82: 803–831.

Rupnick, M., A. Gardner, and J. Glover. 1989. Endothelialization of vascular prosthetic surfaces after seeding or sodding with human microvascular endothelial cells. *J. Vasc. Surg.* 9:788–795.

Schlichting, H. 1979. Boundary Layer Theory, 7th ed. McGraw Hill Book Co., New York.

Schmidt, C. E., A. F. Horwitz, D. A. Lauffenburger, and M. P. Sheetz. 1993. Integrin-cytoskeleton interactions in migrating fibroblasts are dynamic, asymmetric, and regulated. *J. Cell Biol.* 123:977–991.

Torney, D. C., M. Dembo, and G. I. Bell. 1986. Thermodynamics of cell adhesion. II. Freely mobile repeller. *Biophys. J.* 49:501–507.

Truskey, G. A., J. S. Burmeister, E. Grapa, and W. M. Reichert. 1992. Total internal reflection fluorescence microscopy (TIRFM). II. Topographical mapping of relative cell/substratum separation distances. *J. Cell Sci.* 103:491–499.

Truskey, G. A., and J. S. Pirone. 1990. The effect of fluid shear stress upon cell adhesion to fibronectin-treated surfaces. *J. Biomed. Materials Res.* 24:1333–1353.

Truskey, G. A., and T. L. Proulx. 1993. Relationship between 3T3 cell spreading and the strength of adhesion on glass and silane surfaces. *Biomaterials.* 14:243–254.

Wang, N., J. P. Butler, and D. E. Ingber. 1993. Mechanotransduction across the cell surface and through the cytoskeleton. *Science.* 260: 1124–11227.

Ward, M. D., M. Dembo, and D. A. Hammer. 1995. Kinetics of cell detachment: effect of ligand density. *Ann. Biomed. Eng.* 23:322–331.

Ward, M. D., and D. A. Hammer. 1993. A theoretical analysis of the effect of focal contact formation on cell-substrate attachment strength. *Biophys. J.* 64:936–956.

Williams, S. K., D. G. Rose, and B. E. Jarrell. 1994. Microvascular endothelial cell sodding of ePTFE vascular grafts: improved patency and stability of the cellular lining. *J. Biomed. Materials Res.* 28:203–212.